

Charge separation in Reheating after Cosmological Inflation

Thomas Gasenzer, Boris Nowak, and Dénes Sexty

*Institut für Theoretische Physik, Ruprecht-Karls-Universität Heidelberg, Philosophenweg 16, 69120 Heidelberg, Germany and
ExtreMe Matter Institute EMMI, GSI Helmholtzzentrum für Schwerionenforschung GmbH, Planckstraße 1, 64291 Darmstadt, Germany*
(Dated: April 27, 2022)

New aspects of parametrically resonant heating of a relativistic scalar $O(2)$ -symmetric self-interacting field are presented. This process is a candidate for reheating at the end of the early-universe epoch of inflation. Although a model with a fully $O(2)$ -symmetric ground state is used, transient, metastable spontaneous symmetry breaking can be observed. This manifests itself in the form of persistent regimes of opposite and, inside these, uniform charge overdensities separated by thin lines and walls similar to topological defects, in two and three spatial dimensions, respectively. The configuration is found to correspond to an attractive non-equilibrium fixed point of the underlying dynamic equations which prevents thermalisation over an extended period of time.

PACS numbers: 98.80.Cq, 11.10.Wx, 47.27.E-

In cosmological models of the universe, reheating describes the epoch starting at the end of inflation [1]. During this epoch the potential energy of the inflaton field is redistributed into a homogeneous and isotropic hot plasma of particle excitations. These become a substantial part of the further expanding universe. Simple models describing reheating after inflation invoke self-interacting scalar fields. One of the popular scenarios involves the parametrically resonant amplification of quantum fluctuations of the macroscopically oscillating inflaton field. The amplified modes represent the emerging matter content of the universe [2, 3]. Various theoretical approaches have been proposed to model reheating. As both, the inflaton and the amplified modes are strongly populated, classical field simulations can be applied to describe their evolution [4–6]. Alternatively, Kadanoff-Baym dynamic equations, as derived from 2PI effective actions in nonperturbative approximation, can describe the resonant excitation and the ensuing thermalisation [7]. The exponentially fast excitation process is followed by a slower equilibration, possibly with transient turbulent behaviour transporting the energy deposited in the low-momentum modes of the system to higher momenta. Classical field simulations and scaling solutions of kinetic equations were used to analyse possible turbulent evolution during reheating and thermalisation [8, 9]. Recently the interest has been renewed by predictions as well as numerical findings of new exponents characterising the universal turbulent spectra at non-thermal fixed points of the non-perturbative dynamic equations [10–15].

In this paper we demonstrate that these fixed points are characterised by topological excitations of the underlying inflaton field. We study parametric resonance in a globally $O(2)$ or, equivalently, $U(1)$ symmetric relativistic scalar field theory. Shortly after the resonant excitations have set in we find spatial separation of charges. Both, charge and anticharge overdensities become uniformly distributed within slowly varying regions which are separated by sharp boundary walls of grossly invariant thickness. These walls have the character of topological defects and appear for generic initial conditions. As these structures are found to be directly related to critical scaling found in [10] they decay only slowly as the

system is moving away from the non-thermal fixed point.

The action of the model considered here is given by

$$S = \int d^d x dt \left\{ \frac{1}{2} [(\partial_t \varphi)^2 - (\partial_i \varphi)^2 - m^2 \varphi^2] - \frac{\lambda}{4!N} (\varphi^2)^2 \right\} \quad (1)$$

where $\varphi^2 \equiv \varphi_a(x) \varphi_a(x)$, $(\partial_i \varphi)^2 \equiv \partial_i \varphi_a(x) \partial_i \varphi_a(x)$, sums over $i = 1, \dots, d$ and $a = 1, \dots, N$, $N = 2$, implied. To describe the dynamics of the scalar field φ in the rapidly expanding universe one works in conformal coordinates in which the metric is defined through

$$ds^2 = a(t)^2 (dt^2 - dx^2), \quad (2)$$

with a scale parameter $a(t)$ depending on the conformal time t . For vanishing bare mass scale $m^2 = 0$ the equation of motion for the rescaled field $\varphi' = a\varphi$ reads (in $d = 3$):

$$\left[\partial_t^2 - \Delta + \frac{\lambda}{6N} \varphi'^2 - \frac{\ddot{a}}{a} \right] \varphi'_a = 0 \quad (3)$$

During the parametric reheating epoch the universe is close to being radiation dominated [4], such that the scale dependent term can be neglected, $\ddot{a} = 0$. Hence, the equation of motion for the rescaled field $\Phi = \varphi' / \varphi'_0$, with $\varphi'_0 = \varphi'(t = 0)$ the initial value of the inflaton field, can be approximated as

$$\left[\partial_t^2 - \Delta + \Phi^2 \right] \Phi_a = 0 \quad (4)$$

where the coupling has been absorbed by the rescaling $\sqrt{\lambda/6N} \varphi'_0 x \rightarrow x$ and $\sqrt{\lambda/6N} \varphi'_0 t \rightarrow t$. Due to the global $O(2)$ symmetry of the action the charge-current density

$$j_\mu(x) = \Phi_1(x) \partial_\mu \Phi_2(x) - \Phi_2(x) \partial_\mu \Phi_1(x). \quad (5)$$

is conserved, $\partial^\mu j_\mu = 0$.

To induce parametrically resonant reheating, we start our simulation from a configuration where only the zero mode, i.e., the inflaton field is populated, with empty but fluctuating non-zero momentum modes. These quantum fluctuations act as seeds for the ensuing instabilities. Choosing $m^2 = 0$ and $\lambda > 0$, which corresponds to an equilibrium configuration

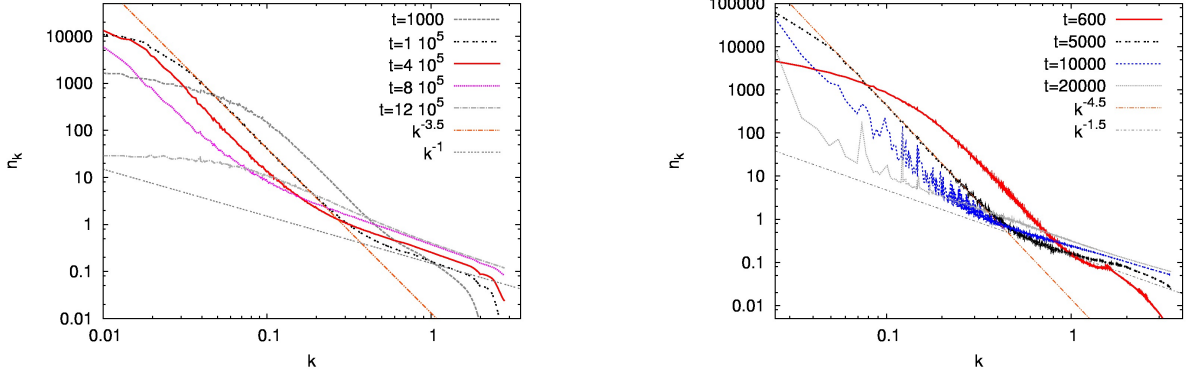


Figure 1: (Color online) The occupation-number spectrum (6) of the system in $d = 2$ (left panel) and $d = 3$ (right) spatial dimensions at different points t (in lattice units) in time. Averages were taken over 69 (84) runs on a 960^2 (256^3) grid. The double-log scale exhibits the bimodal power-law form of $n(k, t) \sim k^{-\kappa}$, corresponding to a constant quasiparticle flow Q in the infrared, $\kappa \simeq d + 1.5$, and thermal scaling, $\kappa \simeq 1$, for large k . For $d = 3$ we also observe, at late times and intermediate momenta, the UV weak wave turbulence exponent $\kappa \simeq 1.5$. See main text for further details.

in the symmetric phase, subsequent oscillation of the inflaton field induces parametrically resonant exponential growth of certain modes. During the further evolution scattering between the excited modes causes the entire spectrum to fill up. Our numerical simulations of eq. (4) were performed on a cubic space-time lattice using leap-frog discretisation and periodic boundary conditions in $d = 2$ and 3 spatial dimensions.

The time evolution of the system after the instabilities have set in was found to be best described by a turbulent stage followed by thermalisation on the largest time scales. The turbulent phases feature universal scaling of the (solid-)angle-averaged momentum-space occupation numbers

$$n(k, t) = \frac{1}{4L^d} \int d^{d-1}\Omega_{\mathbf{k}} \sqrt{\langle |\partial_t \Phi(\mathbf{k}, t)|^2 \rangle \langle |\Phi(\mathbf{k}, t)|^2 \rangle}, \quad (6)$$

where L is the number of gridpoints, with two different exponents as shown in Fig. 1 for $d = 2$ and $d = 3$ at different instances of time t . Note that to get the physical particle number spectrum, one must undo the rescalings, thus in $d = 3$ multiply the above n_k with $6N/\lambda$.

The bimodal scaling was first predicted and observed in simulations in Refs. [10, 13]. From analytical studies based on quantum Boltzmann and perturbative dynamic equations, one expects to find, in the ultraviolet (UV) regime, exponents featuring a dynamical fixed point corresponding to weak wave turbulence [10, 12, 16]. These exponents characterise the power-law behaviour of $n(k, t) \sim k^{-\kappa}$ and correspond to either a constant flow $P(k) \equiv P$ of energy or Q of quasiparticles along the radial direction in momentum space. If the scattering is dominated by interactions between three modes, the resulting exponents are, assuming anomalous exponents to vanish,

$$\kappa_P = d + \frac{3}{2}(z - 2), \quad \kappa_Q = d + z - 3. \quad (7)$$

where z is the homogeneity index of the dispersion $\omega(\mathbf{k}) =$

$s^z \omega(\mathbf{k})$ of mode \mathbf{k} . Note that at the thermal fixed point one expects $\kappa_{th} = z$, corresponding to the Rayleigh-Jeans law.

In the infrared (IR) regime occupation numbers are large and perturbation theory breaks down [10, 12]. Recently, the use of a non-perturbative two-particle irreducible (2PI) approach has been proposed in which bubble-chain diagrams are resummed in the s -channel, corresponding to the next-to-leading order of an expansion in $1/N$. As a result the above exponents are modified in the IR to [11, 12]

$$\kappa_P^{\text{IR}} = d + 2z, \quad \kappa_Q^{\text{IR}} = d + z \quad (8)$$

We note that for the model (1) energy flows with rate P towards larger k while quasiparticles flow with rate Q towards lower k [16]. In our simulations, the initial momentum distribution is found to act as a source at intermediate momenta, $k \simeq 0.1..0.3$, see Fig. 1.

Our relativistic model implies $z = 1$ such that we expect, in the infrared, the exponent $\kappa_Q^{\text{IR}} = d + 1$, assuming a constant quasiparticle number flow towards the IR. We note that in contrast to cases with smaller $1/N$ discussed in [13] we find, in the IR, $\kappa \simeq 3.5$ ($d = 2$) and 4.5 ($d = 3$). Assuming a constant flow P from intermediate momenta towards the UV one expects a wave-turbulent exponent $\kappa_P^{\text{UV}} = d - 3/2$. Numerically we find that in the UV the occupation number distribution approaches, at large times, thermal scaling $\kappa_{th} = 1$. For $d = 3$ we also observe, at late times and intermediate momenta, the expected UV weak wave turbulence exponent $\kappa \simeq 1.5$.

Given the above correspondence between analytical predictions and numerical findings we will, in the following, present our central result: Investigating the real-space structure of the emerging critical configuration we find patterns similar to topological defects giving rise to quasi-stationary charge separation. In Fig. 2 we depict, for $d = 2$, a typical real-space configuration in the turbulent stage, plotting the modulus of the $O(2)$ scalar field, $|\Phi(\mathbf{x}, t)| = [\Phi_1^2(\mathbf{x}, t) + \Phi_2^2(\mathbf{x}, t)]^{1/2}$. Localised regions appear, specifically “defect” lines where the

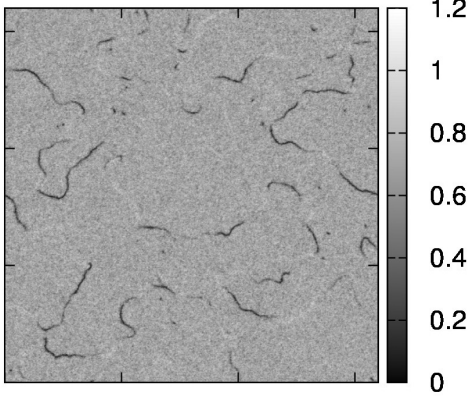


Figure 2: Modulus $|\Phi(\mathbf{x}, t)| = [\Phi_1^2(\mathbf{x}, t) + \Phi_2^2(\mathbf{x}, t)]^{1/2}$ at lattice time $t = 9 \times 10^3$. Shown is its distribution over the two-dimensional 960^2 lattice used in our simulations. “Defect” lines with substantially reduced ρ contrast with a fairly constant bulk $\rho_{\text{bulk}} \approx 0.7$.

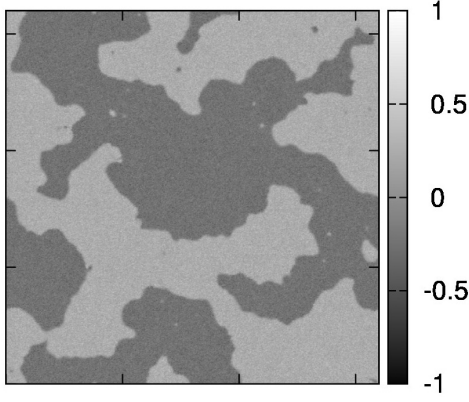


Figure 3: Charge density $\rho(\mathbf{x}, t) = j_0(\mathbf{x}, t)$ (cf. (5)), for the same configuration as shown in Fig. 2. Note the evenly distributed charge overdensities with opposite sign, separated by lines which include the “defect” lines shown in Fig. 2.

absolute value of the field is much smaller than its average. Fig. 3 shows the corresponding charge density distribution $\rho(\mathbf{x}, t) = j_0(\mathbf{x}, t)$, Eq. (5). Clearly, both uniform charge and anti-charge overdensities appear within distinctly separated regions, showing only small fluctuations as compared to their bulk values. This separation of charges is confirmed by the histogram of local charge densities on the lattice shown in Fig. 4. We found similar histograms for the case of the $O(N)$ -symmetric model (1) with $N = 3, 4$ which we will study in more detail in a forthcoming publication.

Moreover, we see that the “defect” lines in Fig. 2 are lying along the boundary limits between the regions of opposite charge. Note that, only part of the boundaries is clearly visible as “defect” lines. Following the time evolution of the defect lines [17] we find that they appear and disappear with a period of $T/2 \approx 6$ determined by the effective mass $m_{\text{eff}} = 2\pi/T$ of the mean field theory, at every point along the boundaries

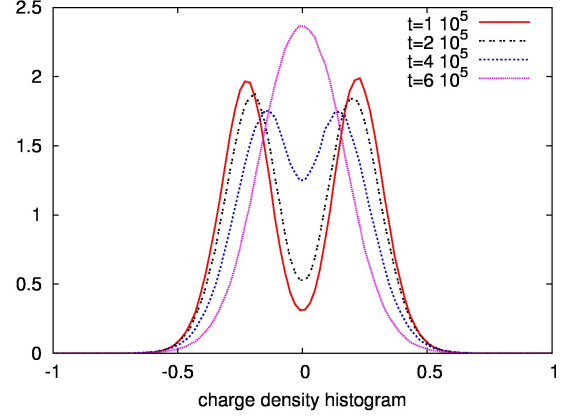


Figure 4: Histogram of the charge density distribution of the system in $d = 2$, at points of time for which Fig. 1 shows the corresponding spectra. We find that a clear charge separation goes together with the strong IR scaling with $\kappa_Q^{\text{IR}} = 3$.

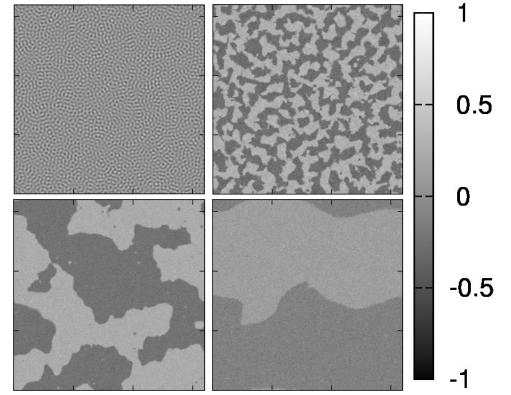


Figure 5: Charge density $\rho(\mathbf{x}, t) = j_0(\mathbf{x}, t)$ (cf. (5)) for the same run as shown in Fig. 3 at the times $t = 300$ (upper left), $t = 10^3$ (upper right), $t = 10^4$ (lower left), $t = 6 \times 10^4$ (lower right). The scale of the largest structures is found not to depend on the total lattice size.

between the oppositely charged domains.

The explanation for the appearance of these lines is as follows: The charge density ρ can be interpreted as the angular momentum of the field in the $N = 2$ dimensional field space. Hence, d -dimensional configuration space can be divided into regions according to the sign of the local charge density. On the lines separating these regions the local field variable has neighbours of opposite charge which therefore possess opposite “circular polarisation” in field space. Thus, at a particular point on the boundary the rotations add to a linear oscillation of the field through zero, giving rise to spatially and temporally oscillating defect lines. While such an evolution could similarly occur in a free theory, with $\lambda = 0$, interactions are responsible for rendering the transition between the opposite charges sharp as can be seen in Fig. 2.

Following the evolution of the system starting from the homogeneous initial configuration we find the defect lines to

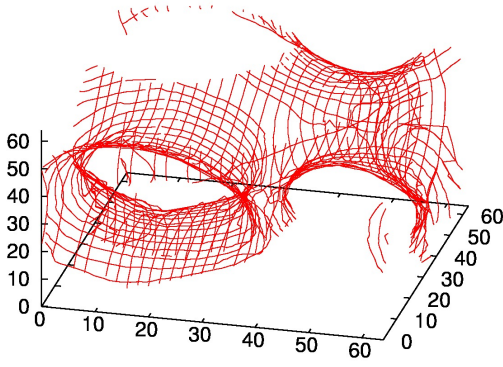


Figure 6: Bubbles of approximately constant and opposite charge separated by thin walls on a 64^3 lattice at $t = 1500$. Plotted are surface lines which are fitted to lattice points having $|\Phi|^2 < 0.05$.

appear once the instability has saturated. The lines can reconnect with each other while they propagate slowly through configuration space, such that the number of spatially connected charged regions changes in time. On the average, the total length of the defect lines as well as the number of connected regions is found to decrease with time, see Fig. 5. During the late stage of the evolution the sharp separation of opposite charges gradually disappears while the system finally thermalises. This can also be seen in the histogram in Fig. 4 where the central well gradually disappears while the spectrum $n(k, t)$ approaches thermal equilibrium, see Fig. 1.

For $d = 3$, starting from an equivalent initial configuration, we find bubbles of opposite charge separated by thin walls (Fig. 6) [17] as well as charge density histograms similar to the case $d = 2$. These bubbles are seen to appear in coincidence with the strong IR scaling in the spectra as shown in the right panel of Fig. 1.

We emphasise that the structures found are distinctly different from the known topological defects appearing in $O(2)$ theories such as vortices in $d = 2$ and vortex strings in $d = 3$ which one obtains for the $O(2)$ model with equilibrium symmetry breaking due to a negative mass-squared term $m^2 < 0$ [6]. The bubble walls reported here form for vanishing or positive mass squared.

Considering a field theory with spontaneous symmetry breaking (SSB), one can classify topological defects and texture configurations of the theory according to the homotopy groups of the order parameter space M . As we chose $m^2 \geq 0$, no SSB would be expected such that M is trivial. Our findings suggest however that topological defects occur according to the homotopy group of the charge density space C . For the $O(2)$ model one has $C = \mathcal{R}$, and our charge density histogram suggests that the system remains, during a long period, within the subspace topologically equivalent to $S_0 = \{-1, 1\}$. Hence one expects to see configurations separated by defect lines (walls) into regions corresponding to the two unconnected parts of C .

Considering other potential cosmological consequences of our findings, notice that, in a different context, the $U(1)$ -symmetric scalar field theory can also be understood as an ingredient of the Affleck-Dine baryogenesis scenario [18], where the scalar field carries a baryon charge and is thought to be a supersymmetric partner of standard-model fields. We emphasize that, in contrast to such models, there is no symmetry breaking implemented in our model from the outset. The breaking rather occurs as a dynamical, transient but quasi-stationary effect, with the system evolving dynamically into a state where the positive and negative charges cluster, while keeping a zero net charge.

To summarize, we have studied parametric reheating in an $O(2)$ symmetric scalar field theory in two and three spatial dimensions. We have found structures similar to topological defects to emerge on intermediate time scales, breaking charge symmetry locally while the classical action with $m^2 \geq 0$ implies an equilibrium configuration without symmetry breaking. It is an interesting question which we defer to a subsequent publication whether similar structures exist in more complicated theories, such as gauge theories.

The authors would like to thank J. Berges, J. M. Pawłowski, and M. G. Schmidt for inspiring discussions. They acknowledge the support by the Deutsche Forschungsgemeinschaft, the University of Heidelberg (FRONTIER), the Alliance Program of the Helmholtz Association (HA216/EMMI), by BMBF and MWFK Baden-Württemberg (bwGRiD cluster).

-
- [1] R. Allahverdi, R. Brandenberger, F. Y. Cyr-Racine and A. Mazumdar, *Ann. Rev. Nucl. Part. Sci.* **60**, 27 (2010).
 - [2] L. Kofman, A. D. Linde and A. A. Starobinsky, *Phys. Rev. Lett.* **73**, 3195 (1994).
 - [3] J. H. Traschen and R. H. Brandenberger, *Phys. Rev. D* **42**, 2491 (1990).
 - [4] S. Y. Khlebnikov and I. I. Tkachev, *Phys. Rev. Lett.* **77**, 219 (1996).
 - [5] T. Prokopec and T. G. Roos, *Phys. Rev. D* **55**, 3768 (1997).
 - [6] I. Tkachev, S. Khlebnikov, L. Kofman and A. D. Linde, *Phys. Lett. B* **440**, 262 (1998).
 - [7] J. Berges and J. Serreau, *Phys. Rev. Lett.* **91**, 111601 (2003).
 - [8] R. Micha and I. I. Tkachev, *Phys. Rev. Lett.* **90**, 121301 (2003).
 - [9] R. Micha and I. I. Tkachev, *Phys. Rev. D* **70**, 043538 (2004).
 - [10] J. Berges, A. Rothkopf and J. Schmidt, *Phys. Rev. Lett.* **101**, 041603 (2008).
 - [11] J. Berges and G. Hoffmeister, *Nucl. Phys. B* **813**, 383 (2009).
 - [12] C. Scheppach, J. Berges and T. Gasenzer, *Phys. Rev. A* **81**, 033611 (2010).
 - [13] J. Berges and D. Sexty, *Phys. Rev. D* **83**, 085004 (2011).
 - [14] M. E. Carrington and A. Rebhan, *arXiv:1011.0393 [hep-ph]*.
 - [15] B. Nowak, D. Sexty and T. Gasenzer, *Phys. Rev. B* **84**, 020506(R) (2011).
 - [16] V. E. Zakharov, V. S. L'vov, and G. Falkovich, *Kolmogorov Spectra of Turbulence I: Wave Turbulence* (Springer-Verlag, Berlin, 1992).
 - [17] For videos of the evolution see <http://www.thphys.uni-heidelberg.de/sextty/videos>
 - [18] I. Affleck and M. Dine, *Nucl. Phys. B* **249**, 361 (1985).